Version 0.1 DRAFT

ATLAS+CMS DARK MATTER FORUM RECOMMENDATIONS

Author/contributor list to be added as document is finalized.

May 6, 2015

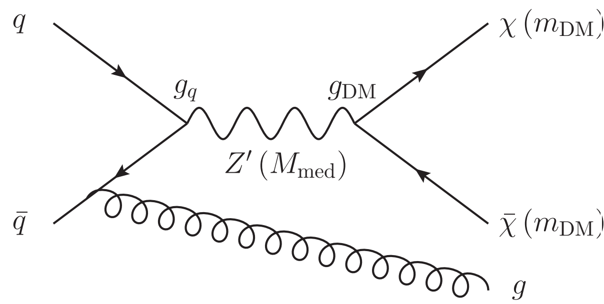

Figure 1.1: The diagram shows the pair production of dark matter particles in association with a parton from the initial state via an s-channel vector or axial-vector mediator. The process if specified by ($M_{\rm med}$, $m_{\rm DM}$, $g_{\rm DM}$, $g_{\rm q}$), the mediator and dark matter masses, and the mediator couplings to dark matter and quarks respectively.

1

Recommended models for all MET+X analyses

1.1 Vector and axial vector mediator, s-channel exchange

There are several matrix element implementations of the s-channel vector mediated DM production. This is available in POWHEG, MADGRAPH and also MCFM. The implementation in POWHEG generates DM pair production with 1 parton at next-to-leading order (NLO), whilst MADGRAPH and MCFM are at leading order (LO). As shown in POWHEG Ref. [HKR13], including NLO corrections result in an enhancement in the cross section as compared to LO and though this is not significant, it does lead to a substantial reduction in the dependence on the choice of the renormalization and factorization scale and hence the theoretical uncertainty on the signal prediction. Since NLO calculations are available for the process in POWHEG, we recommend to proceed with POWHEG as the generator of choice.

We consider the case of a dark matter particle that is a Dirac fermion and where the production proceeds via the exchange of a spin-1 *s*-channel mediator. We consider the following interactions between the DM and SM fields including a vector mediator with:

(a) vector couplings to DM and SM,

(b) axial-vector couplings to DM and SM.

The corresponding Lagrangians are

$$\mathcal{L}_{\text{vector}} = \sum_q g_{\text{q}} Z'_\mu \bar{q}\gamma^\mu q + g_{\text{DM}} Z'_\mu \bar{\chi}\gamma^\mu \chi \tag{1.1}$$

$$\mathcal{L}_{\text{axial-vector}} = \sum_q g_{\text{q}} Z'_\mu \bar{q}\gamma^\mu \gamma^5 q + g_{\text{DM}} Z'_\mu \bar{\chi}\gamma^\mu \gamma^5 \chi \tag{1.2}$$

where the coupling extends over all the quarks and universal couplings are assumed for all the quarks. It is also possible to consider another model in which mixed vector and axial-vector couplings are considered, for instance the couplings to the quarks are vector whereas those to DM are axial-vector. As a starting point, we consider only the models with the vector couplings only and axial vector couplings only.

We assume that no additional visible or invisible decays contribute to the width of the mediator, this is referred to as the minimal width and it is defined as follows for the vector and axial-vector models.

$$\Gamma_{\text{min}} = \Gamma_{\bar{\chi}\chi} + \sum_q \Gamma_{\bar{q}q} \tag{1.3}$$

where the individual contributions to this from the partial width are from

$$\Gamma^{\text{V}}_{\bar{\chi}\chi} = \frac{g_{\text{DM}}^2 M_{\text{med}}}{12\pi}\left(1 + \frac{2m_{\text{DM}}^2}{M_{\text{med}}^2}\right)\sqrt{1 - \frac{4m_{\text{DM}}^2}{M_{\text{med}}^2}} \tag{1.4}$$

$$\Gamma^{\text{V}}_{\bar{q}q} = \frac{3g_{\text{q}}^2 M_{\text{med}}}{12\pi}\left(1 + \frac{2m_q^2}{M_{\text{med}}^2}\right)\sqrt{1 - \frac{4m_q^2}{M_{\text{med}}^2}} \tag{1.5}$$

$$\Gamma^{\text{A}}_{\bar{\chi}\chi} = \frac{g_{\text{DM}}^2 M_{\text{med}}}{12\pi}\left(1 - \frac{4m_{\text{DM}}^2}{M_{\text{med}}^2}\right)^{3/2} \tag{1.6}$$

$$\Gamma^{\text{A}}_{\bar{q}q} = \frac{3g_{\text{q}}^2 M_{\text{med}}}{12\pi}\left(1 - \frac{4m_q^2}{M_{\text{med}}^2}\right)^{3/2} . \tag{1.7}$$

Note the color factor 3 in the quark terms. Figure 1.2 shows the minimal width as a function of mediator mass for both vector and axial-vector mediators assuming couplings of 1. With this choice of the couplings, the dominant contribution to the minimal width comes from the quarks due to the color factor enhancement.

The simplified models described here have four free parameters: mediator mass M_{med}, Dark Matter mass m_{DM}, coupling of the mediator to quarks g_{q} and coupling of the mediator to Dark Matter g_{DM}. In order to determine an optimal choice of the parameter grid for presentation of the early Run-2 results, dependencies of the kinematic quantities and cross sections on the individual parameters need to be studied. The following paragraphs list the main observations from

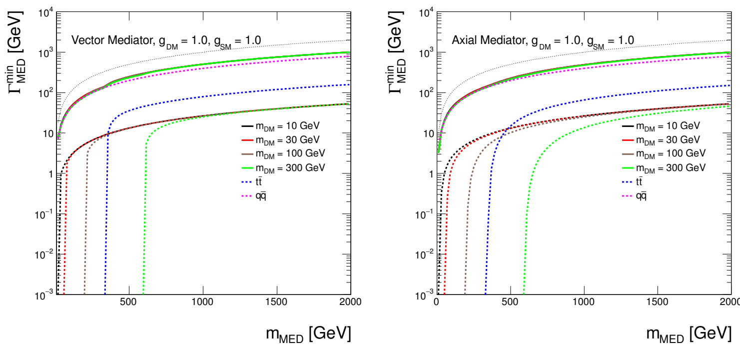

Figure 1.2: Minimal width as a function of mediator mass for vector and axial-vector mediator assuming couplings of 1. The total width is shown as solid lines for Dark Matter masses of 10 GeV, 30 GeV, 100 GeV and 300 GeV in black, red, brown and green, respectively. The individual contributions from Dark Matter are indicated by dotted lines with the same colors. The contribution from all quarks but top is shown as magenta dotted line and the contribution from top quarks only is illustrated by the dotted blue line. The dotted black line shows the extreme case $\Gamma_{\rm min} = M_{\rm med}$.

the scans over the parameters that support the final proposal for the parameter grid.

Scan over the couplings Figure 1.3 reveals there are no differences in the shape of the $\not\!\!E_T$ distribution among the samples where the pair of 10 GeV Dark Matter particles are produced on-shell from the mediator of 1 TeV, generated with different choice of the coupling strength. The considered coupling values range from 0.1 to 1.45, where the latter value approximates the maximum allowed coupling value, holding $g_{\rm q} = g_{\rm DM}$, such that $\Gamma_{\rm min} < M_{\rm med}$. Based on similar plots for different choices of mediator and Dark Matter masses, it is concluded that the shapes of kinematic distributions are not altered neither for the on-shell Dark Matter production where $M_{\rm med} > 2m_{\rm DM}$, nor for the off-shell Dark Matter production where $M_{\rm med} < 2m_{\rm DM}$. Only the cross sections change. Differences in kinematic distributions are expected only close to the transition region where both on-shell and off-shell regimes mix.

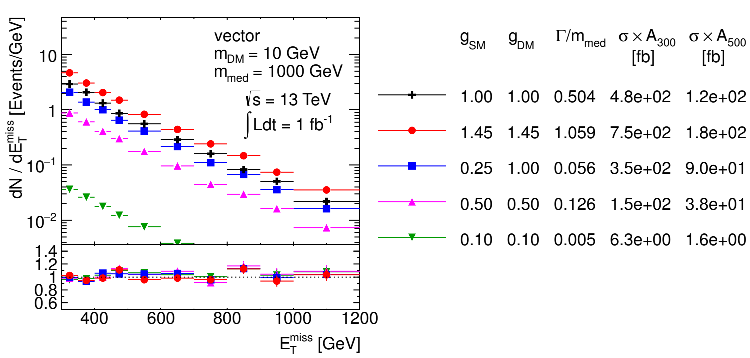

Figure 1.3: Scan over couplings. The $\not\!\!E_T$ distribution is compared for the vector mediator models using the parameters as indicated. Ratios of the normalized distributions with respect to the first one are shown. A_{300} and A_{500} in the table denote the acceptance of the $\not\!\!E_T > 300$ GeV and $\not\!\!E_T > 500$ GeV cut, respectively.

The only place where special care needs to be taken are extremely heavy and narrow mediators, in other words with low couplings. Figure 1.4 suggests a change in the shape of the $\not\!\!E_T$ distribution for 5 TeV mediator once $\Gamma_{\rm min}/M_{\rm med}$ gets down to the order of percent or below. This, however, does not come from physics as it is a feature of the generator implementation, where a cutoff for the regions far away from the mediator mass is often used. This is illustrated in Fig. 1.5 showing the invariant mass of the Dark Matter pair in the samples generated for 7 TeV mediator with different coupling strength. In all cases, it is expected to observe a peak around the mediator mass with a tail extending to $m_{\bar{\chi}\chi} \to 0$, significantly enhanced by parton distribution functions at low Bjorken x. For coupling strength 1 and 3, the massive enhancement at $m_{\bar{\chi}\chi} \to 0$ implies the resonant production at $m_{\bar{\chi}\chi} = 7$ TeV is statistically suppressed such that barely any events are generated there. However, for narrower mediators with couplings below 1, the peak around 7 TeV is clearly visible in the generated sample and the dominant tail at $m_{\bar{\chi}\chi} \to 0$ is artificially cut off, leading to unphysical cross section predictions and kinematic shapes. This explains why the sample with the narrowest mediator in Fig. 1.4 is heavily suppressed in terms of production cross section and also gives different $\not\!\!E_T$ shape. In general, for such extreme parameter choices the EFT model should give the correct answer. **[TODO: add results of ongoing study.]**

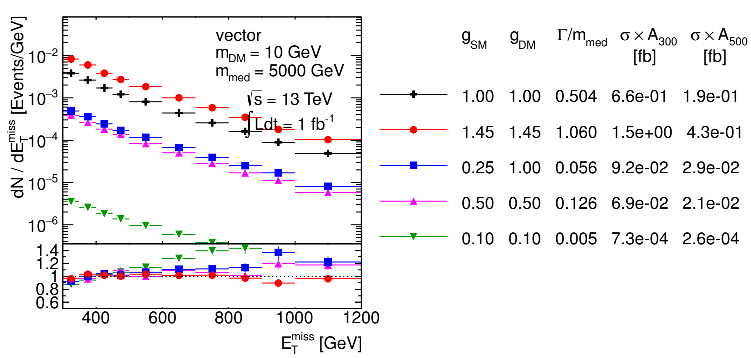

Figure 1.4: Scan over couplings. The $\not\!\!E_T$ distribution is compared for the vector mediator models using the parameters as indicated. Ratios of the normalized distributions with respect to the first one are shown. A_{300} and A_{500} in the table denote the acceptance of the $\not\!\!E_T > 300$ GeV and $\not\!\!E_T > 500$ GeV cut, respectively.

Scan over the Dark Matter mass For the fixed mediator mass and couplings, both the cross section and the kinematic distributions remain similar for different Dark Matter masses as long as $M_{\text{med}} > 2m_{\text{DM}}$. This is illustrated in Fig. 1.6 on an example of 1 TeV mediator and Dark Matter masses ranging from 10 GeV to 300 GeV. It is observed that the cross section decreases as the Dark Matter mass reaches closer to $M_{\text{med}}/2$. Once the Dark Matter pair is produced off-shell, the cross section of such simplified model is suppressed and the $\not\!\!E_T$ spectrum hardens, as demonstrated with the choice of 1 TeV Dark Matter in the same plot. Figure 1.7 reveals the $\not\!\!E_T$ spectrum hardens further with increasing Dark Matter mass, accompanied by the gradual decrease of the cross section. From these observations one can conclude:

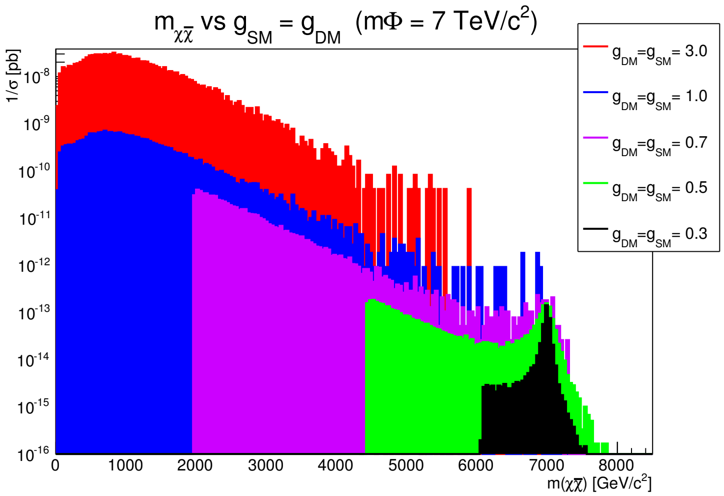

Figure 1.5: Invariant mass of the Dark Matter pair in the samples with $M_{\text{med}} = 7\,\text{TeV}$ and different coupling strengths.

- A coarse binning along m_{DM} is sufficient at $M_{\text{med}} \gg 2m_{\text{DM}}$.
- Finer binning is needed in order to capture the changes in the cross section and kinematic quantities close to the production threshold on both sides around $M_{\text{med}} = 2m_{\text{DM}}$.
- Due to the significant cross section suppression of the off-shell Dark Matter pair production, it is not necessary to populate the parameter space $M_{\text{med}} \ll 2m_{\text{DM}}$ since the LHC is not going to be able to probe the models there.

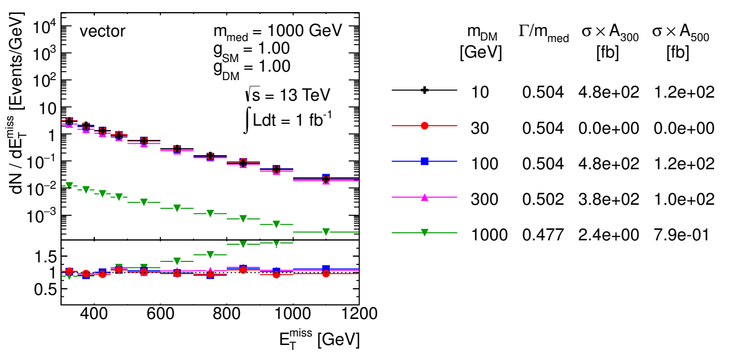

Figure 1.6: Scan over Dark Matter mass. The $\not{E}_T$ distribution is compared for the vector mediator models using the parameters as indicated. Ratios of the normalized distributions with respect to the first one are shown. A_{300} and A_{500} in the table denote the acceptance of the $\not{E}_T > 300\,\text{GeV}$ and $\not{E}_T > 500\,\text{GeV}$ cut, respectively.

Scan over the mediator mass Changing the mediator mass for fixed Dark Matter mass and couplings leads to significant differences in cross section and shapes of the kinematic variables for $M_{\text{med}} > 2m_{\text{DM}}$ as shown in Fig. 1.8. As expected, higher mediator masses lead to harder $\not{E}_T$ spectra. On the other hand, the $\not{E}_T$ shapes are similar in the off-shell Dark Matter production regime as well as no dramatic differences in cross sections are observed, which is illustrated

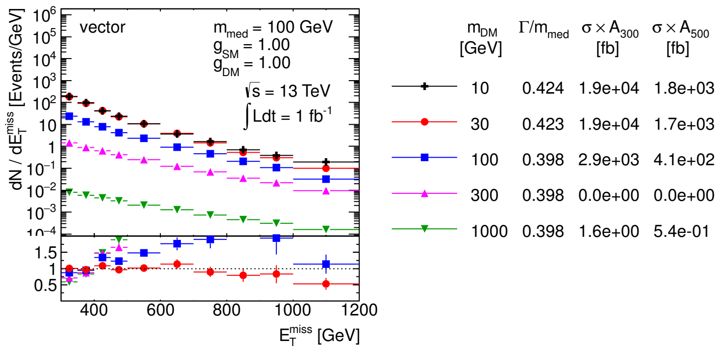

Figure 1.7: Scan over Dark Matter mass. The $\not{E}_T$ distribution is compared for the vector mediator models using the parameters as indicated. Ratios of the normalized distributions with respect to the first one are shown. A_{300} and A_{500} in the table denote the acceptance of the $\not{E}_T > 300\,\text{GeV}$ and $\not{E}_T > 500\,\text{GeV}$ cut, respectively.

in Fig. 1.9. Therefore, a coarse binning along m_{DM} is sufficient at $M_{\text{med}} \ll 2m_{\text{DM}}$.

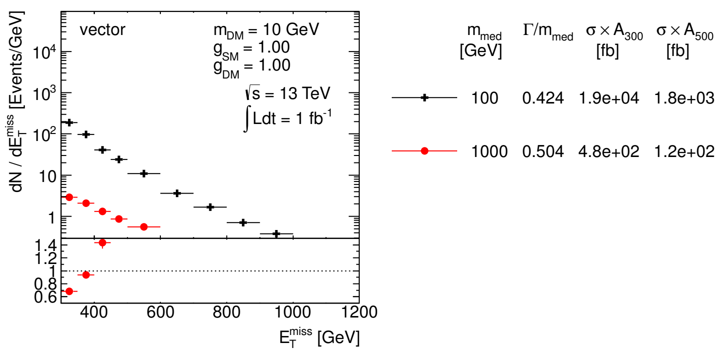

Figure 1.8: Scan over mediator mass. The $\not{E}_T$ distribution is compared for the vector mediator models using the parameters as indicated. Ratios of the normalized distributions with respect to the first one are shown. A_{300} and A_{500} in the table denote the acceptance of the $\not{E}_T > 300\,\text{GeV}$ and $\not{E}_T > 500\,\text{GeV}$ cut, respectively.

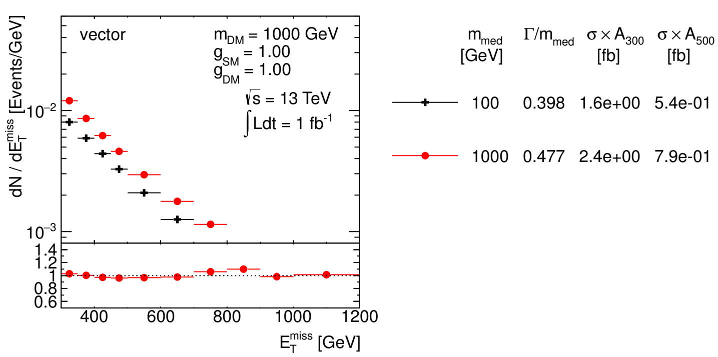

Figure 1.9: Scan over mediator mass. The $\not{E}_T$ distribution is compared for the vector mediator models using the parameters as indicated. Ratios of the normalized distributions with respect to the first one are shown. A_{300} and A_{500} in the table denote the acceptance of the $\not{E}_T > 300\,\text{GeV}$ and $\not{E}_T > 500\,\text{GeV}$ cut, respectively.

Proposed parameter grid Based on the observations above, the following proposal is made for the presentation of the early Run-2 results from the LHC:

(a) Give results in the M_{med}–m_{DM} plane for a particular choice of the couplings.

(b) Give results in the g_{q}–g_{DM} plane for a particular choice of the masses.

We choose to display the results in the M_{med}–m_{DM} plane for the choice of the couplings $g_{\mathrm{q}} = g_{\mathrm{DM}} = 1$. In order to motivate the highest mediator mass grid point, the expected sensitivity of Run-2 LHC data needs to be taken into account. The expected upper limit at 95% confidence level on the product of cross section, acceptance and efficiency, $\sigma \times A \times \epsilon$, in the final Run-1 ATLAS mono-jet analysis [A$^+$15] is 51 fb and 7.2 fb for $\not{E}_T > 300\,\mathrm{GeV}$ and $\not{E}_T > 500\,\mathrm{GeV}$, respectively. The ATLAS 14 TeV prospects [ATL14] predict twice better sensitivity with the first 5 fb^{-1} of data already. Given the cross section for V+jets processes increases by roughly a factor 2 when going from $\sqrt{s} = 8\,\mathrm{TeV}$ to 13 TeV, similar fiducial cross section limits can be expected with the first Run-2 data as from the final Run-1 analysis. The generator level cross section times the acceptance at $\not{E}_T > 500\,\mathrm{GeV}$ for the model with couplings $g_{\mathrm{q}} = g_{\mathrm{DM}} = 1$, light Dark Matter of 10 GeV and 1 TeV vector mediator is at the order of 100 fb, i.e. the early Run-2 mono-jet analysis is going to be sensitive to heavier mediators than this. The value of $\sigma \times A$ at $\not{E}_T > 500\,\mathrm{GeV}$ for 5 TeV vector mediator is at the order of 0.1 fb, therefore this model probably lies beyond the reach of the LHC. Based on these arguments, the following M_{med} grid points are chosen, roughly equidistant in the logarithmic scale: 10 GeV, 20 GeV, 50 GeV, 100 GeV, 200 GeV, 300 GeV, 500 GeV, 1000 GeV and 2000 GeV. Given the fact that significant changes in cross section happen around the $M_{\mathrm{med}} = 2m_{\mathrm{DM}}$ threshold, the m_{DM} grid points are taken at approximately $M_{\mathrm{med}}/2$, namely: 10 GeV, 50 GeV, 150 GeV, 500 GeV and 1000 GeV. Points on the on-shell diagonal are always chosen to be 5 GeV away from the threshold, to avoid numerical instabilities in the event generation. The detailed studies of the impact of the parameter changes on the cross section and kinematic distributions presented earlier in this section support removing some of the grid points and rely on interpolation. The optimised grids proposed for the vector and axial-vector mediators are given in Table. 1.1, containing 29 mass points each. One point at very high mediator mass (5 TeV) is added for each of the DM masses scanned, to aid the reinterpretation of results in terms of contact interaction operators (EFTs).

m_{DM} (GeV)	m_{med} (GeV)									
1	10	20	50	100	200	300	500	1000	2000	5000
10	10	15	50	100						5000
50	10		50	95	200	300				5000
150	10				200	295	500			5000
500	10						500	995	2000	5000
1000	10							1000	1995	5000

Table 1.1: Simplified model benchmarks for $s-$channel simplified models (spin-1 mediators decaying to Dirac DM fermions in the V and A case, taking the minimum width for $g_{\mathrm{q}} = g_{\mathrm{DM}} = 1$)

The presentation of the results in the g_{q}–g_{DM} plane for fixed masses benefits from cross section scaling and is discussed in Section 1.3.

1.2 Scalar and pseudoscalar mediator, s-channel exchange

One of the most simple UV complete extensions of the effective field theory approach is the addition of a scalar/pseudoscalar mediator between DM and SM. A gauge singlet mediator can have tree-level interactions with a singlet DM particle that is either a Dirac or Majorana fermion, or DM that is a scalar itself. The spin-0 mediator can either be a real or complex scalar; a complex scalar contains both scalar and pseudoscalar particles, whereas the real field only contains the scalar particle. In this document we consider only two of the possible choices for this simplified model: one where the interaction with the SM is mediated by a real scalar, and the second where we consider only a light pseudoscalar, assuming that the associated scalar is decoupled from the low-energy spectrum. The kinematics of the two cases is sufficiently different to suggest that further investigation of the complex scalar case is needed but left for future studies.

Couplings to the SM fermions can be arranged by mixing with the SM Higgs. Such models have interesting connections with Higgs physics, and can be viewed as generalizations of the Higgs portal to DM. The most general scalar mediator models will have renormalizable interactions between the SM Higgs and the new scalar ϕ or pseudoscalar a, as well as ϕ/a interactions with electroweak gauge bosons. Such interactions are model dependent, often subject to constraints from electroweak precision tests, and would suggest specialized searches which cannot be generalized to a broad class of models (unlike, for instance, the $\not{E}_T$ + jets searches). As a result, for this class of minimal simplified models with spin-0 mediators, we will focus primarily on couplings to fermions and loop-induced couplings to gluons.

Minimal Flavor Violation (MFV) implies that scalar couplings to fermions will be proportional to the fermion mass. However, they can differ for up- and down-type quarks and for charged leptons.

Following the assumption that DM is a fermion χ, which couples to the SM only through a scalar ϕ or pseudoscalar a, the most general tree-level Lagrangians compatible with the MFV assumption are [CRTW14, ADR+14, BFG15]:

$$\begin{aligned}
\mathcal{L}_{\text{fermion},\phi} &= \mathcal{L}_{\text{SM}} + i\bar{\chi}\partial\!\!\!/\chi + m_\chi\bar{\chi}\chi + \left|\partial_\mu\phi\right|^2 + \frac{1}{2}m_\phi^2\phi^2 + \\
&\quad g_\chi\phi\bar{\chi}\chi + \frac{\phi}{\sqrt{2}}\sum_i\left(g_u y_i^u\bar{u}_i u_i + g_d y_i^d\bar{d}_i d_i + g_\ell y_i^\ell\bar{\ell}_i\ell_i\right)\,, \qquad (1.8) \\
\mathcal{L}_{\text{fermion},a} &= \mathcal{L}_{\text{SM}} + i\bar{\chi}\partial\!\!\!/\chi + m_\chi\bar{\chi}\chi + \left|\partial_\mu a\right|^2 + \frac{1}{2}m_a^2a^2 + \\
&\quad ig_\chi a\bar{\chi}\gamma_5\chi + \frac{ia}{\sqrt{2}}\sum_i\left(g_u y_i^u\bar{u}_i\gamma_5 u_i + g_d y_i^d\bar{d}_i\gamma_5 d_i + g_\ell y_i^\ell\bar{\ell}_i\gamma_5\ell_i\right) \qquad (1.9)
\end{aligned}$$

Here the sums run over the all SM generations; the Yukawa couplings y_i^f are normalized to $y_i^f = \sqrt{2}m_i^f/v$ where $v \simeq 246\,\text{GeV}$ represents the Higgs vacuum expectation value (VEV). We parametrise the DM-mediator coupling as g_χ, without any additional Yukawa structure between the mediator and the dark sector.

As already stated we only choose a minimal set of interactions that do not include interactions with the Higgs field. For simplicity, we also assume universal SM-mediator couplings $g_v = g_u = g_d = g_\ell$

Given these simplifications, the minimal set of parameters under consideration is

$$\left\{m_\chi,\ m_{\phi/a},\ g_\chi,\ g_{\text{q}}\right\}\,. \qquad (1.10)$$

The matrix element implementation of the s-channel spin-0 mediated DM production is available in POWHEG with the full top-loop calculation at LO [HR15].

We choose to consider minimal mediator width given by Eq. 1.3, where the individual contributions follow from

$$\Gamma^{\text{S}}_{\bar{\chi}\chi} = \frac{g_{\text{DM}}^2 M_{\text{med}}}{8\pi}\left(1 - \frac{4m_{\text{DM}}^2}{M_{\text{med}}^2}\right)^{3/2} \qquad (1.11)$$

$$\Gamma^{\text{S}}_{\bar{q}q} = \frac{3g_{\text{q}}^2 M_{\text{med}}}{8\pi}\frac{m_q^2}{v^2}\left(1 - \frac{4m_q^2}{M_{\text{med}}^2}\right)^{3/2} \qquad (1.12)$$

$$\Gamma^{\text{P}}_{\bar{\chi}\chi} = \frac{g_{\text{DM}}^2 M_{\text{med}}}{8\pi}\sqrt{1 - \frac{4m_{\text{DM}}^2}{M_{\text{med}}^2}} \qquad (1.13)$$

$$\Gamma^{\text{P}}_{\bar{q}q} = \frac{3g_{\text{q}}^2 M_{\text{med}}}{8\pi}\frac{m_q^2}{v^2}\sqrt{1 - \frac{4m_q^2}{M_{\text{med}}^2}}\,. \qquad (1.14)$$

The minimal width for scalar and pseudo-scalar mediators with $g_{\text{q}} = g_{\text{DM}} = 1$ are shown in Fig. 1.10, illustrating the effect of the Higgs-like Yukawa couplings. For the mediator masses above twice the top quark mass m_t, the minimal width receives the dominant contribution from the top quark. For lighter mediator masses, Dark Matter dominates as the couplings to lighter quarks are Yukawa

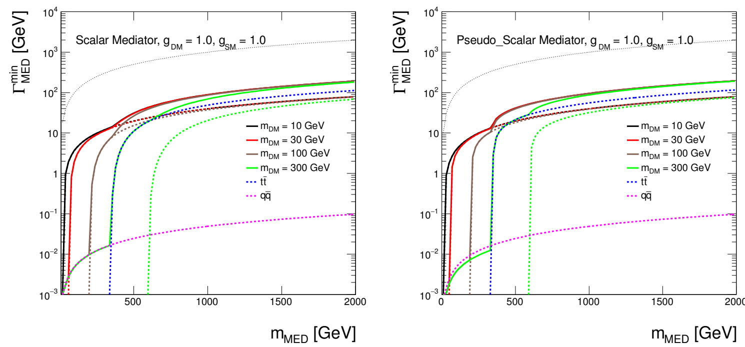

Figure 1.10: Minimal width as a function of mediator mass for scalar and pseudo-scalar mediator assuming couplings of 1. The total width is shown as solid lines for Dark Matter masses of 10 GeV, 30 GeV, 100 GeV and 300 GeV in black, red, brown and green, respectively. The individual contributions from Dark Matter are indicated by dotted lines with the same colors. The contribution from all quarks but top is shown as magenta dotted line and the contribution from top quarks only is illustrated by the dotted blue line. The dotted black line shows the extreme case $\Gamma_{\rm min} = M_{\rm med}$.

suppressed. Note that we decide to ignore the partial width coming from gluons through loops as it can be safely neglected [HR15].

Similarly as in the case of the vector and axial-vector mediators, scans in the parameter space are performed also for the scalar and pseudo-scalar mediators in order to decide on the optimised parameter grid for the presentation of Run-2 results. Figures 1.11- 1.15 show the scans over the couplings, Dark Matter mass and mediator mass and the same conclusions apply as in Section 1.1.

Since the top quark gives the dominant contribution to the mediator width due to Higgs-like Yukawa couplings, the effect of the top channel opening in the mediator production was studied in addition. Scan over the mediator mass is shown in Fig. 1.15 where the mediator masses 300 GeV and 500 GeV are chosen to be below and above $2m_t$. The off-shell Dark Matter production regime is assumed by taking $m_{\rm DM} = 1$ TeV in order to allow studying solely the effects of the couplings to quarks. No differences in the kinematic distributions are observed and also the cross sections remain similar in this case. Therefore, it is concluded that no significant changes appear for mediator masses around the $2m_t$ threshold.

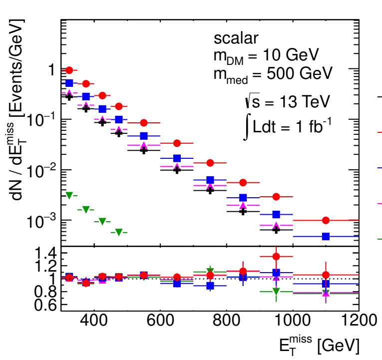

g_{SM}	g_{DM}	Γ/m_{med}	$\sigma\times A_{300}$ [fb]	$\sigma\times A_{500}$ [fb]
1.00	1.00	0.062	3.3e+01	4.0e+00
2.00	2.00	0.248	1.1e+02	1.4e+01
2.00	1.00	0.129	6.0e+01	7.5e+00
1.00	2.00	0.181	3.9e+01	5.0e+00
0.10	0.10	0.001	3.5e-01	4.4e-02

Figure 1.11: Scan over couplings. The $\not\!\!E_T$ distribution is compared for the scalar mediator models using the parameters as indicated. Ratios of the normalized distributions with respect to the first one are shown. A_{300} and A_{500} in the table denote the acceptance of the $\not\!\!E_T > 300$ GeV and $\not\!\!E_T > 500$ GeV cut, respectively.

The optimized parameter grid in the $M_{\rm med}$–$m_{\rm DM}$ plane for scalar and pseudo-scalar mediators is motivated by similar arguments as

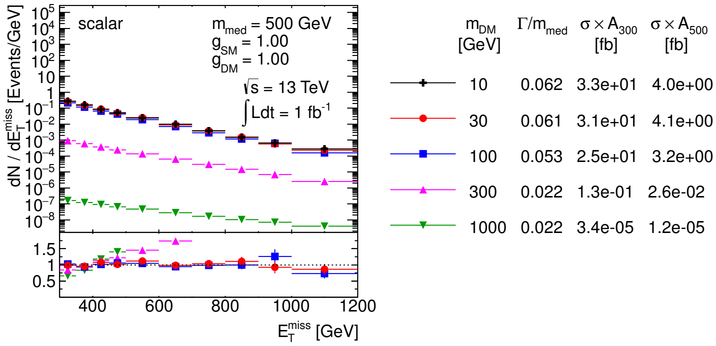

Figure 1.12: Scan over Dark Matter mass. The $\not{E}_T$ distribution is compared for the scalar mediator models using the parameters as indicated. Ratios of the normalized distributions with respect to the first one are shown. A_{300} and A_{500} in the table denote the acceptance of the $\not{E}_T > 300\,\text{GeV}$ and $\not{E}_T > 500\,\text{GeV}$ cut, respectively.

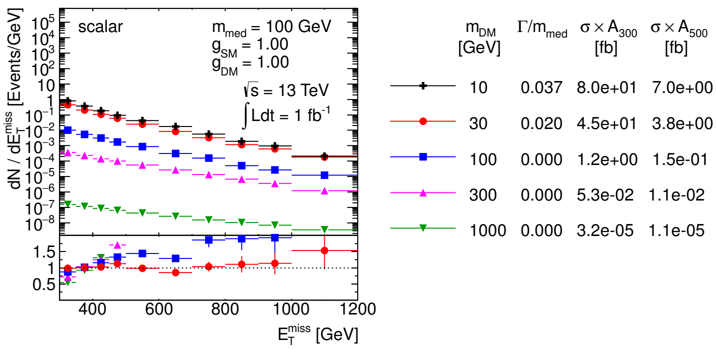

Figure 1.13: Scan over Dark Matter mass. The $\not{E}_T$ distribution is compared for the scalar mediator models using the parameters as indicated. Ratios of the normalized distributions with respect to the first one are shown. A_{300} and A_{500} in the table denote the acceptance of the $\not{E}_T > 300\,\text{GeV}$ and $\not{E}_T > 500\,\text{GeV}$ cut, respectively.

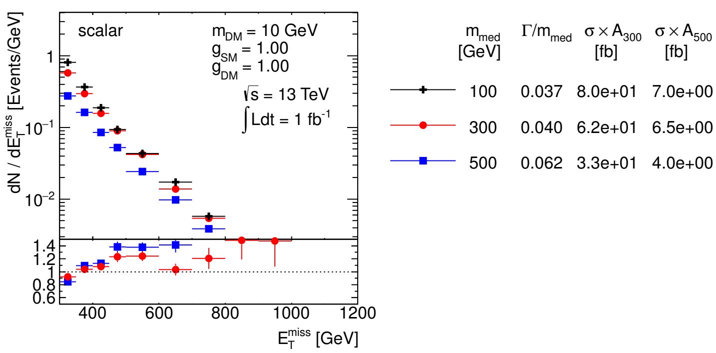

Figure 1.14: Scan over mediator mass. The $\not{E}_T$ distribution is compared for the scalar mediator models using the parameters as indicated. Ratios of the normalized distributions with respect to the first one are shown. A_{300} and A_{500} in the table denote the acceptance of the $\not{E}_T > 300\,\text{GeV}$ and $\not{E}_T > 500\,\text{GeV}$ cut, respectively.

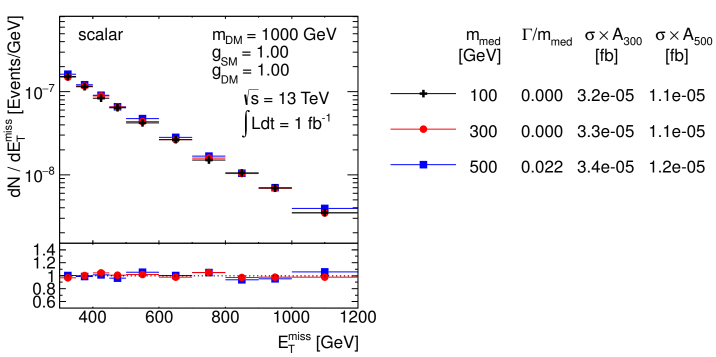

Figure 1.15: Scan over mediator mass. The $\not{E}_T$ distribution is compared for the scalar mediator models using the parameters as indicated. Ratios of the normalized distributions with respect to the first one are shown. A_{300} and A_{500} in the table denote the acceptance of the $\not{E}_T > 300\,\text{GeV}$ and $\not{E}_T > 500\,\text{GeV}$ cut, respectively.

in the previous section. Therefore, a similar pattern is followed here, taking again $g_{\mathrm{q}} = g_{\mathrm{DM}} = 1$. Only the sensitivity to the highest mediator masses has to be revisited. The generator level cross section times the acceptance at $\not{E}_T > 500\,\mathrm{GeV}$ for the model with couplings $g_{\mathrm{q}} = g_{\mathrm{DM}} = 1$, light Dark Matter of 10 GeV and 500 GeV scalar mediator is at the order of 10 fb, i.e. just at the edge of the early Run-2 sensitivity. Increasing the mediator mass to 1 TeV pushes the product $\sigma \times A$ down to approximately 0.1 fb, beyond the LHC sensitivity. Therefore, we choose to remove the 2 TeV mediator mass from the grid and present the final grid with 26 mass points only in Fig. 1.2. One point at very high mediator mass (5 TeV) is added for each of the DM masses scanned, to aid the reinterpretation of results in terms of contact interaction operators (EFTs).

m_{DM} (GeV)	m_{med} (GeV)								
1	10	20	50	100	200	300	500	1000	5000
10	10	15	50	100					5000
50	10		50	95	200	300			5000
150	10				200	295	500		5000
500	10						500	995	5000
1000	10							1000	5000

Table 1.2: Simplified model benchmarks for $s-$channel simplified models (spin-0 mediators decaying to Dirac DM fermions in the scalar and pseudoscalar case, taking the minimum width for $g_{\mathrm{q}} = g_{\mathrm{DM}} = 1$)

The proposal for the scan in the g_{q}–g_{DM} plane is described in the following section.

1.3 *Cross section scaling*

The aim of the parameter grid optimization is to find out whether certain parts of the parameter space can be omitted and one can rely on the neighboring grid points in order to populate the missing parts. There are two ways of doing this:

- Interpolation is used in-between the grid points that are close enough such that finer granularity is not needed for the presentation purposes, or between the points where smooth or no changes of the results are expected. The latter argument is exactly the one that motivates the reduction of the grid points in the M_{med}–m_{DM} plane.

- Recalculation of the results can be used when the dependencies with respect to the neighboring grid points are known.

The results of the scan over the couplings presented in the previous sections indicate there are no changes in kinematic distributions for different choices of the coupling strengths. This means that the acceptance remains the same in the whole g_{q}–g_{DM} plane and it is sufficient to perform the detector simulation only for one single grid point. The resulting truth-level selection acceptance and the detector reconstruction efficiency can then be applied to all remaining grid points in the g_{q}–g_{DM} plane where only the generator-level cross section needs to be known. This significantly reduces the computing time as the detector response is by far the most expensive part of the Monte Carlo sample production. However, a further step can be taken if a parameterization of the cross section dependence from one grid point to another exists, in which case the number of generated samples can be reduced even further.

Let us now elaborate on a cross section scaling procedure. The propagator on the s-channel exchange is written in a Breit-Wigner form as $\frac{1}{\sqrt{s}-M_{\mathrm{med}}^2+iM_{\mathrm{med}}\Gamma}$. The relative size of the center-of-mass energy defined by the two partons entering the hard process and the mediator mass allows to classify the production in the following way:

- off-shell production when $\sqrt{s} \gg M_{\mathrm{med}}$ leading to suppressed cross sections,
- on-shell production when $\sqrt{s} \sim M_{\mathrm{med}}$ leading to enhanced cross sections,
- effective field theory (EFT) limit when $\sqrt{s} \ll M_{\mathrm{med}}$.

All three categories can be distinguished in Fig. 1.16 showing the upper limit on the interaction scale $M^* \equiv M_{\mathrm{med}}/\sqrt{g_{\mathrm{q}}g_{\mathrm{DM}}}$ for vector mediator. In the case of the off-shell production and the EFT limit, the first term in the propagator dominates which reduces the dependence on the mediator width. Therefore, in these cases one can approximate the cross section as

$$\sigma \propto g_{\mathrm{q}}^2 g_{\mathrm{DM}}^2. \tag{1.15}$$

The on-shell production regime is the most interesting one as it gives the best chances for a discovery at the LHC given the cross section enhancement. The propagator term with the width cannot be neglected in this case and, in the narrow width approximation, one can integrate

$$\int \frac{ds}{(s-M_{\mathrm{med}}^2)^2 + M_{\mathrm{med}}^2\Gamma^2} = \frac{\pi}{M_{\mathrm{med}}\Gamma} \tag{1.16}$$

which further implies the cross section scaling

$$\sigma \propto \frac{g_{\mathrm{q}}^2 g_{\mathrm{DM}}^2}{\Gamma}. \tag{1.17}$$

Since $\Gamma \sim g_{\rm q}^2 + g_{\rm DM}^2$, one can simplify this rule in the extreme cases as follows

$$\sigma \quad \propto \quad \frac{g_{\rm q}^2 g_{\rm DM}^2}{g_{\rm q}^2 + g_{\rm DM}^2} \xrightarrow{g_{\rm q} \ll g_{\rm DM}} g_{\rm q}^2 \tag{1.18}$$

$$\sigma \quad \propto \quad \frac{g_{\rm q}^2 g_{\rm DM}^2}{g_{\rm q}^2 + g_{\rm DM}^2} \xrightarrow{g_{\rm q} \gg g_{\rm DM}} g_{\rm DM}^2 \,. \tag{1.19}$$

However, it is important to keep in mind that there is no simple scaling rule for how the cross section changes with the Dark Matter mass, mediator mass and the mediator width because PDFs matter in such cases as well. Therefore, the scaling procedure outlined above is expected to work only for fixed masses and fixed mediator width.

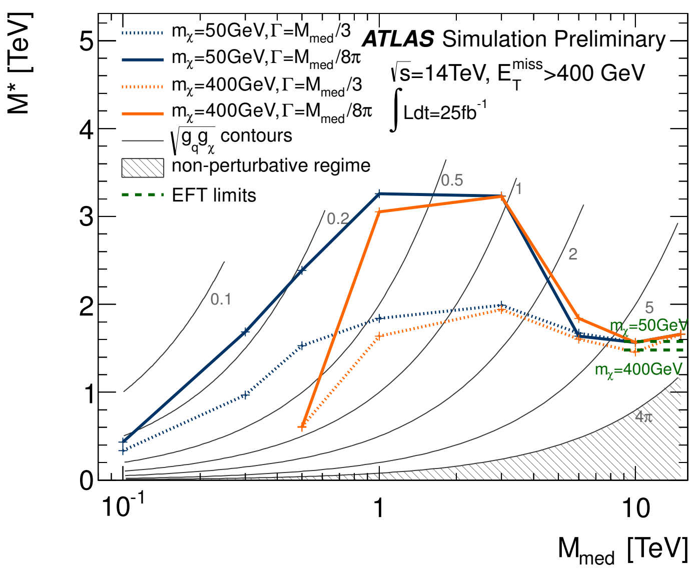

Figure 1.16: Comparison of the 95% CL lower limits on the scale of the interaction of a Z'-like simplified model at 14 TeV, in terms of the mediator mass. Corresponding limits from EFT models are shown on the same plot as green dashed lines to show equivalence between the two models for high mediator masses. Taken from Ref. [ATL14].

Figures 1.17 and 1.18 show the minimal width in the $g_{\rm q}$–$g_{\rm DM}$ plane for all vector, axial-vector, scalar and pseudo-scalar mediators for $M_{\rm med} = 100\,{\rm GeV}$ and 1000 GeV, respectively, taking $m_{\rm DM} = 10\,{\rm GeV}$. The individual colors indicate the lines of constant width along which the cross section scaling works. For vector and axial-vector mediators, the minimal width is predominantly defined by $g_{\rm q}$ due to the number of quark flavors and the color factor. On the contrary, both the Standard Model and Dark Matter partial width have comparable contributions in case of scalar and pseudo-scalar mediators if the top quark channel is open ($M_{\rm med} > 2m_t$). However, mostly $g_{\rm DM}$ defines the minimal width for $M_{\rm med} < 2m_t$ due to the Yukawa-suppressed light quark couplings.

The performance of the cross section scaling is demonstrated in Fig. 1.19 where the mass point $M_{\rm med} = 1\,{\rm TeV}$ and $m_{\rm DM} = 10\,{\rm GeV}$

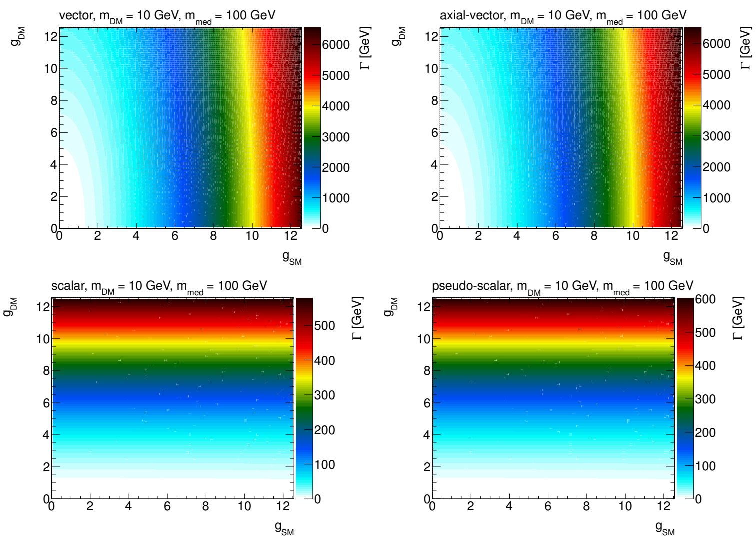

Figure 1.17: Minimal width for vector, axial-vector, scalar and pseudo-scalar mediators as a function of the individual couplings g_q and g_{DM}, assuming $M_{med} = 100\,\text{GeV}$ and $m_{DM} = 10\,\text{GeV}$.

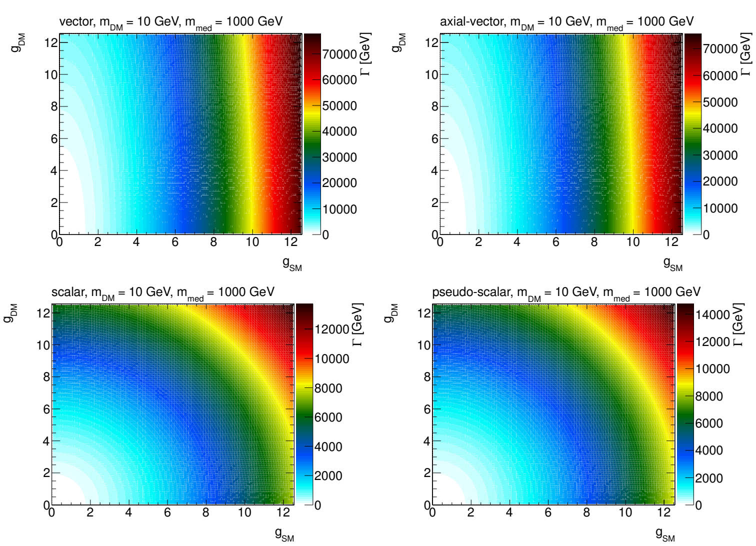

Figure 1.18: Minimal width for vector, axial-vector, scalar and pseudo-scalar mediators as a function of the individual couplings g_q and g_{DM}, assuming $M_{med} = 1\,\text{TeV}$ and $m_{DM} = 10\,\text{GeV}$.

is chosen and rescaled from the starting point $g_q = g_{DM} = 1$ according to Eq. 1.17 to populate the whole g_q–g_{DM} plane. This means the width is not kept constant in this test and this is done in purpose in order to point out deviations from the scaling when the width is altered. For each mass point, the rescaled cross section is compared to the generator cross section and the ratio of the two is plotted. For the given choice of the mass points, the scaling seems to work approximately with the precision of $\sim 20\%$ in the region where $\Gamma_{min} < M_{med}$. Constant colors indicate the lines along which the cross section scaling works precisely and there is a remarkable resemblance of the patterns shown in the plots of the mediator width. To prove the scaling along the lines of constant width works, one such line is chosen in Fig. 1.20 for a scalar mediator, defined by $M_{med} = 300$ GeV, $m_{DM} = 100$ GeV, $g_q = g_{DM} = 1$, and the rescaled and generated cross sections are found to agree within 3%.

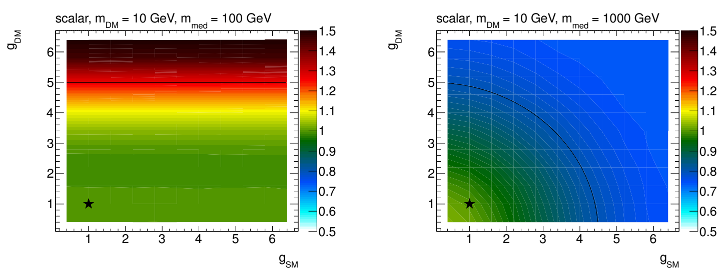

Figure 1.19: Ratio of the rescaled and generated cross sections in the g_q–g_{DM} plane. The point at $g_q = g_{DM} = 1$, taken as a reference for the rescaling, is denoted by a star symbol. Scalar model with $M_{med} = 100$ GeV (left) and 1 TeV (right) is plotted for $m_{DM} = 10$ GeV. The limiting case $\Gamma_{min} = M_{med}$ is shown as a black line.

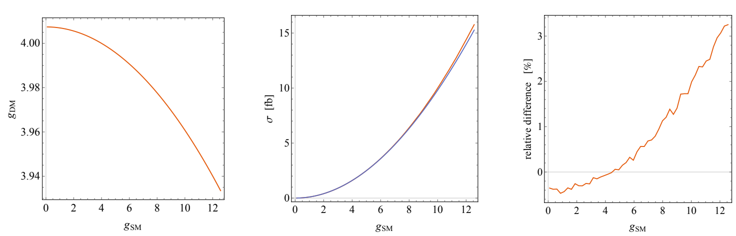

Figure 1.20: Scaling along the lines of constant width. The line of constant width for $M_{med} = 300$ GeV and $m_{DM} = 100$ GeV, intercepting $g_q = g_{DM} = 4$ is shown on left. The generated and rescaled cross sections are compared in the middle, the corresponding ratio is shown on right.

Proposed parameter grid We propose to present the results in the g_q–g_{DM} plane using the following prescription:

- Since the shapes of kinematic quantities do not change for different couplings, use the acceptance and efficiency for the available $m_{DM} = 50$ GeV, $M_{med} = 300$ GeV, $g_q = g_{DM} = 1$ grid point from the M_{med}–m_{DM} plane for the scalar and pseudo-scalar mediator. In case of the vector and axial-vector mediator, use the grid point $m_{DM} = 50$ GeV, $M_{med} = 1$ TeV, $g_q = g_{DM} = 1$.
- Generate additional samples in order to get generator cross sections only. For scalar and pseudo-scalar mediator, choose $m_{DM} =$

50 GeV, $M_{\rm med} = 300$ GeV with the following values for $g_{\rm q} = g_{\rm DM}$: 0.1, 2, 3, 4, 5, 6. For vector and axial vector mediator, choose $m_{\rm DM} = 50$ GeV, $M_{\rm med} = 1$ TeV with the following values for $g_{\rm q} = g_{\rm DM}$: 0.1, 0.25, 0.5, 0.75, 1.25, 1.5. The upper values are defined by the minimal width reaching the mediator mass.

- Rescale the generator cross sections along the lines of constant width in order to populate the whole $g_{\rm q}$–$g_{\rm DM}$ plane.

Rescaling to different mediator width In general there may be an interest to consider larger mediator masses than $\Gamma_{\rm min}$ in order to accommodate further couplings of the mediator. The cross section scaling method described above can be used to reinterpret the results presented for the minimal width, since multiplying the width by factor n is equivalent to changing the coupling strength by factor $\sqrt{n}$, i.e.

$$\sigma(g_{\rm q}, g_{\rm DM}, n\Gamma_{\rm min}(g_{\rm q}, g_{\rm DM})) \propto \frac{g_{\rm q}^2 g_{\rm DM}^2}{\Gamma_{\rm min}(\sqrt{n}g_{\rm q}, \sqrt{n}g_{\rm DM})} \,. \tag{1.20}$$

The cross section for the sample with couplings $g_{\rm q}$ and $g_{\rm DM}$ and modified mediator width $\Gamma = n\Gamma_{\rm min}$ can therefore be rescaled from a sample generated with the minimal width corresponding to the couplings scaled by $\sqrt{n}$ as described in the following formula.

$$\sigma(g_{\rm q}, g_{\rm DM}, n\Gamma_{\rm min}(g_{\rm q}, g_{\rm DM})) = \frac{1}{n^2}\sigma(\sqrt{n}g_{\rm q}, \sqrt{n}g_{\rm DM}, \Gamma_{\rm min}(\sqrt{n}g_{\rm q}, \sqrt{n}g_{\rm DM})) \tag{1.21}$$

Advantage of doing this is again in the fact that no event selection and detector response needs to be simulated since the changes in couplings do not have an effect on the shapes of kinematic distributions.

1.3.1 POWHEG settings

This section describes specific settings for the Dark Matter models needed to run the POWHEG generation.

- The POWHEG implementation allows to generate a single sample that provides sufficient statistics in all mono-jet analysis signal regions. POWHEG generates weighted events and the `bornsuppfact` parameter is used to set the event suppression factor according to

$$F(k_{\rm T}) = \frac{k_{\rm T}^2}{k_{\rm T}^2 + \texttt{bornsuppfact}^2} \,. \tag{1.22}$$

  In this way, the events at low $\not\!\!E_T$ are suppressed and receive higher event weights which ensures higher statistics at high $\not\!\!E_T$. We recommend to set `bornsuppfact` to 1000.

- The bornktmin parameter allows to suppress the low $\not{E}_T$ region even further by starting the generation at a certain value of k_{T}. It is recommended to set this parameter to half the lower analysis $\not{E}_T$ cut, therefore the proposed value for bornktmin is 150.
- Set runningwidth to 0.
- Set mass_low and mass_high to -1.
- The minimal values for ncall1, itmx1, ncall2, itmx2 are 250000, 5, 1000000, 5 for the DMV model, respectively. In order to increase speed, set foldsci and foldy to 2 and keep foldphi at 1.
- The minimal values for ncall1, itmx1, ncall2, itmx2 are 100000, 5, 100000, 5 for the DMS_tloop model, respectively.
- Allow negative weights for the DMV model by setting withnegweights to 1.
- Since the DMS_tloop model is a leading order process, set LOevents and bornonly are set to 1 internally.

1.4 *Colored scalar mediator, t-channel exchange*

An alternative set of simplified models exist where the mediator is exchanged in the *t*-channel, thereby coupling the quark and dark matter particle directly. Under the assumption that χ is a Standard Model (SM) singlet, the mediating particle, labeled ϕ, is necessarily charged and coloured. This model is parallel to, and partially motivated by, the squark of the MSSM, but in this case the χ is chosen to be Dirac. Following the example of Ref. [PVZ14], the interaction Lagrangian is written as

$$\mathcal{L}_{\mathrm{int}} = g \sum_{i=1,2,3} (\phi_L^i \bar{Q}_L^i + \phi_{uR}^i \bar{u}_R^i + \phi_{dR}^i \bar{d}_R^i)\chi \qquad (1.23)$$

(Note: [PVZ14] uses only i = 1,2, but I think it's fine to extend this to 3 here.) where Q_L^i, u_R^i and d_R^i are the SM quarks and ϕ_L^i, ϕ_{uR}^i and ϕ_{dR}^i are the corresponding mediators, which (unlike the *s*-channel mediators) must be heavier than χ. These mediators have SM gauge representations under $(SU(3), SU(2))_Y$ of $(3,2)_{-1/6}$, $(3,1)_{2/3}$ and $(3,1)_{-1/3}$ respectively. Variations of the model previously studied include coupling to the left-handed quarks only [CEHL14, BDSJ+14], to the ϕ_{uR}^i [DNRT13] or ϕ_{dR}^i [PVZ14, A+14], or some combination [BB13, AWZ14].

Minimal Flavour Violation (MFV) requires that the mediator masses for each flavour be equal; the same logic also applies to the couplings g. The available parameters are then

$$\{m_\chi,\, M_\phi,\, g\}. \tag{1.24}$$

In practice, the third mediator mass and coupling could be separated from the other two, if higher order corrections to the MFV prediction arise due to the large top Yukawa coupling – a common variation is then to define this split between the first two generations and the third, so the parameters are extended to

$$\{m_\chi,\, M_{\phi_{1,2}},\, M_{\phi_3},\, g_{1,2},\, g_3\}. \tag{1.25}$$

The width of each mediator is expressed, using the example of decay to an up quark, as

$$\begin{aligned}\Gamma(\phi_i \to \bar{u}_i \chi) = {} & \frac{g_i^2}{16\pi M_{\phi_i}^3}(M_{\phi_i}^2 - m_{u_i}^2 - m_\chi^2) \\ & \times \sqrt{M_{\phi_i}^4 + m_{u_i}^4 + m_\chi^4 - 2M_{\phi_i}^2 m_{u_i}^2 - 2M_{\phi_i}^2 m_\chi^2 - 2m_{u_i}^2 m_\chi^2}\,,\end{aligned} \tag{1.26}$$

this reduces to

$$\frac{g_i^2 M_{\phi_i}}{16\pi}\left(1 - \frac{m_\chi^2}{M_{\phi_i}^2}\right)^2 \tag{1.27}$$

in the limit $M_{\phi_i}, m_\chi \gg m_{u_i}$.

An interesting point of difference with the s-channel simplified models is that the mediator can radiate a SM object, such as a jet or gauge boson, thus providing three separate mono-X diagrams which must be considered together in calculations. This model can also give a signal in the di-jet + MET channel when, for example, the χ is exchanged in the t-channel and the resulting ϕ pair each decay to a jet + χ.

2

Specific models for signatures with heavy flavor quarks

2.1 $t\bar{t}$+MET models

As described in Section 1.2, a model with a scalar/pseudoscalar particle mediating the DM-SM interactions is one of the simplest UV completions of our EFT models.

The expected signal of DM pair production depends on the production rate defined by the dark matter mass m_χ, mediator $m_{\phi/a}$, on the couplings g_i and on the branching ration defined by the total decay width of the mediator ϕ/a. We calculate the minimum possible width (assuming only decays into the dark matter and the Standard Model fermions) that is consistent with a given value of $g_\chi g_{\mathrm{SM}}$. These are given by Eq. (2.1) [BFG15].

$$\begin{aligned} \Gamma_{\phi,a} = & \sum_f N_c \frac{y_f^2 g_v^2 m_{\phi,a}}{16\pi} \left(1 - \frac{4m_f^2}{m_{\phi,a}^2}\right)^{3/2} + \frac{g_\chi^2 m_{\phi,a}}{8\pi} \left(1 - \frac{4m_\chi^2}{m_{\phi,a}^2}\right)^{3/2} \\ & + \frac{\alpha_s^2 y_t^2 g_v^2 m_{\phi,a}^3}{32\pi^3 v^2} \left| f_{\phi,a}\left(\frac{4m_t^2}{m_{\phi,a}^2}\right)\right|^2 \end{aligned} \tag{2.1}$$

where

$$f_\phi(\tau) = \tau \left[1 + (1-\tau)\arctan^2\left(\frac{1}{\sqrt{\tau - 1}}\right)\right] , \qquad f_a(\tau) = \tau \arctan^2\left(\frac{1}{\sqrt{\tau-1}}\right) . \tag{2.2}$$

The first term in each width corresponds to the decay into SM fermions, and the sum runs over all kinematically available fermions, $N_c = 3$ for quarks and $N_c = 1$ for leptons. The second term is the decay into DM, assuming that is kinematically allowed. The factor of two between the decay into SM fermions and into DM is a result of our choice of normalization of the Yukawa couplings due to spin dependencies. The last two terms correspond to decay into gluons. Since we have assumed that $g_v = g_u = g_d = g_\ell$, we have included in the partial decay widths $\Gamma(\phi/a \to gg)$ only the contributions stemming from top loops, which provide the by far largest corrections given that $y_t \gg y_b$ etc. At the loop level the mediators can decay not only to gluons but also to pairs of photons and other final states if kinematical accessible. However the decay rates $\Gamma(\phi/a \to gg)$ are always larger than the other loop-induced partial widths, and in consequence the total decay widths $\Gamma_{\phi/a}$ are well approximated by the corresponding sum of the individual partial decay widths involving DM, fermion or gluon pairs. It should be noted that if $m_{\phi/a} > 2m_t$ the total widths of ϕ/a will typically be dominated by the partial widths to top quarks.

2.1.1 Parameter scan

As discussed in Sec. 1.2, the MFV assumption for spin-0 mediators leads to quark mass dependent Yukawa couplings, and therefore dominant couplings to top quarks. This motivates dedicated DM+$t\bar{t}$ searches. The benchmark chosen for these searches follows the assumptions mentioned in the previous Section: we consider a Dirac fermion DM particle, universal couplings to quarks, and minimum mediator width.

The benchmark points scanning the model parameters have been selected to ensure that the kinematic features of the parameter space are sufficiently represented. Detailed studies were performed to identify points in the m_{DM}, $m_{\phi,a}$, g_{DM}, g_v (and $\Gamma_{\phi,a}$) parameter space that differ significantly from each other in terms of expected detector acceptance. Because missing transverse momentum is the key observable for searches, the mediator p_T spectra is taken to represent the main kinematics of a model. Another consideration in determining the set of benchmarks is to focus on the phase space where we expect the searches to be sensitive during the 2015 LHC run. Based on a projected integrated luminosity of $30\,\mathrm{fb}^{-1}$ expected for 2015, we disregard model points with a cross section times branching ratio smaller than 0.1 fb.

2.1.2 Parameter scan

The kinematics is most dependent on the masses m_{DM} and $m_{\phi,a}$. Figure 2.1 and 2.2 show typical dependencies for scalar and pseudoscalar couplings respectively.

The two relevant thresholds that are observed for the variation in the kinematic spectra are $m_{\phi,a} = 2m_{\mathrm{DM}}$ and $m_{\phi,a} = 2m_t$. When the mediator mass exceeds both these thresholds then the p_T spectra broadens with larger $m_{\phi,a}$ and the kinematics for ϕ and a are comparable. The mediator p_T spectra changes significantly when crossing these thresholds. In particular, the kinematics are different for an on-shell mediator compared to an off-shell mediator ($m_{\phi,a} < 2m_{\mathrm{DM}}$).

Furthermore, the scalar case differs from the pseudoscalar one when $m_\phi < 2m_t$. Therefore, it is important to have benchmark points covering both sides of these thresholds with sufficient granularity.

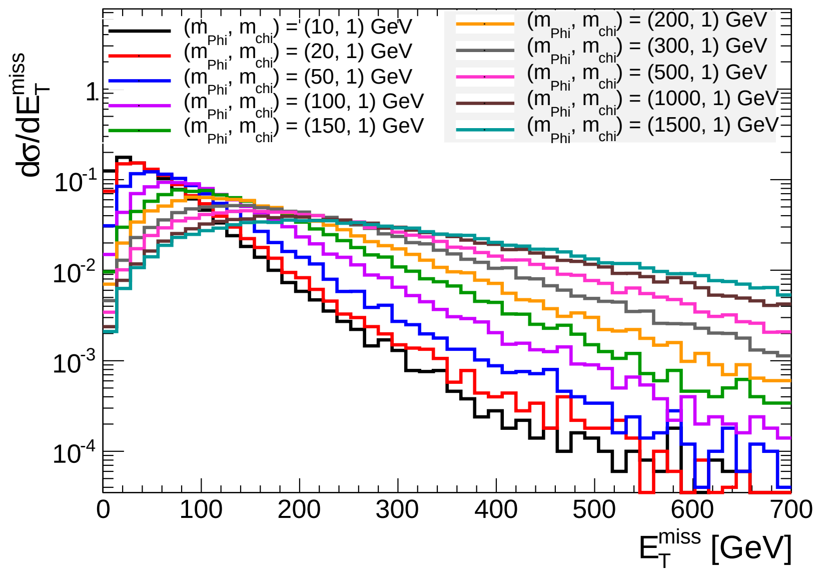

Figure 2.1: Example of the dependence of the kinematics on the scalar mediator mass. The Dark Matter mass is fixed to be 1GeV.

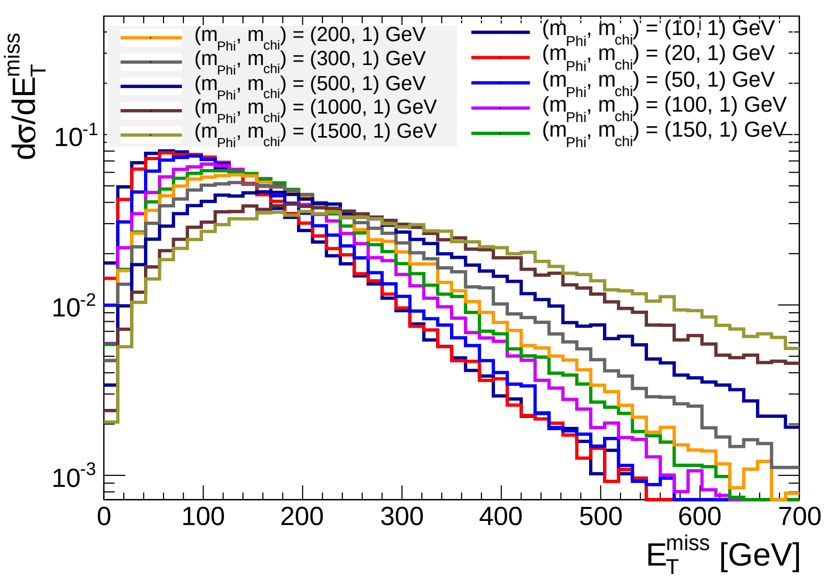

Figure 2.2: Example of the dependence of the kinematics on the pseudoscalar mediator mass. The Dark Matter mass is fixed to be 1GeV.

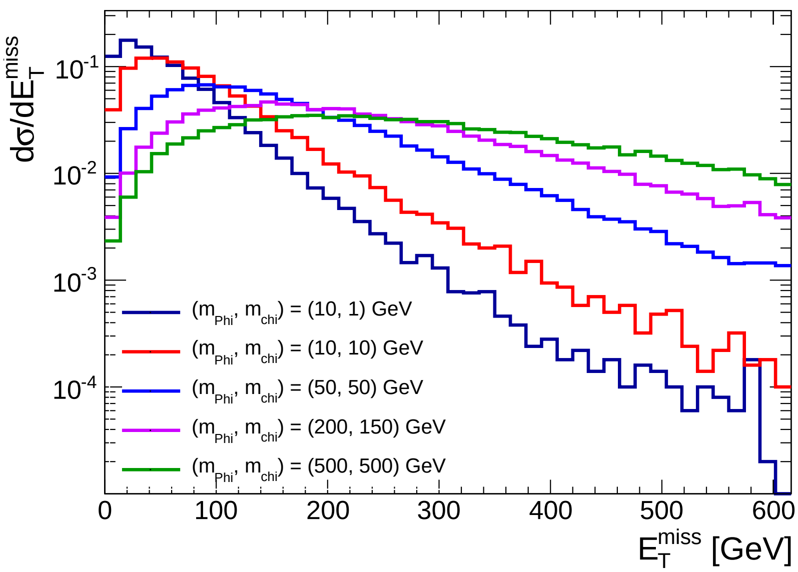

Figure 2.3: Example of the dependence of the kinematic for points of the grid proposed in Tab. 1.2 close to the $m_{\phi,a} \sim 2m_\chi$ limit.3

Typically only weak dependencies on width or equivalently couplings are observed (see Fig 2.4), except for large mediator masses of $\sim 1.5\,\text{TeV}$ or for very small couplings of $\sim 10^{-2}$. These regimes where width effects are significant have production cross sections that are too small to be relevant for $30\,\text{fb}^{-1}$ and are not considered here. However, with the full Run-2 dataset, such models may be within reach. The weak dependence on the typical width values can be understood as the parton distribution function are the dominant effect on mediator production. In other words, for couplings $\sim O(1)$ the width is large enough that the p_T of the mediator is determined mainly by the PDF.

Another case where the width can impact the kinematics is when $m_{\phi,a}$ is slightly larger than $2m_\chi$. Here, the width determines the relative contribution between on-shell and off-shell production. An example is given in Fig. 2.5. In our recommendations we propose to use for simplicity the minimal width, as this is represents the most conservative choice to interpret the LHC results. **[TODO: mention larger widths too]**

Given that the kinematics are similar for all couplings $\sim O(1)$, we recommend to generate only samples with $g_{\text{DM}} = g_v = 1$. It follows from this that these benchmark points should be a good approximation for non-unity couplings and for $g_{\text{DM}} \neq g_v$, provided that the sample is rescaled to the appropriate cross section times branching ratio. While a simple scaling function **[CD: which?]** is sufficient for

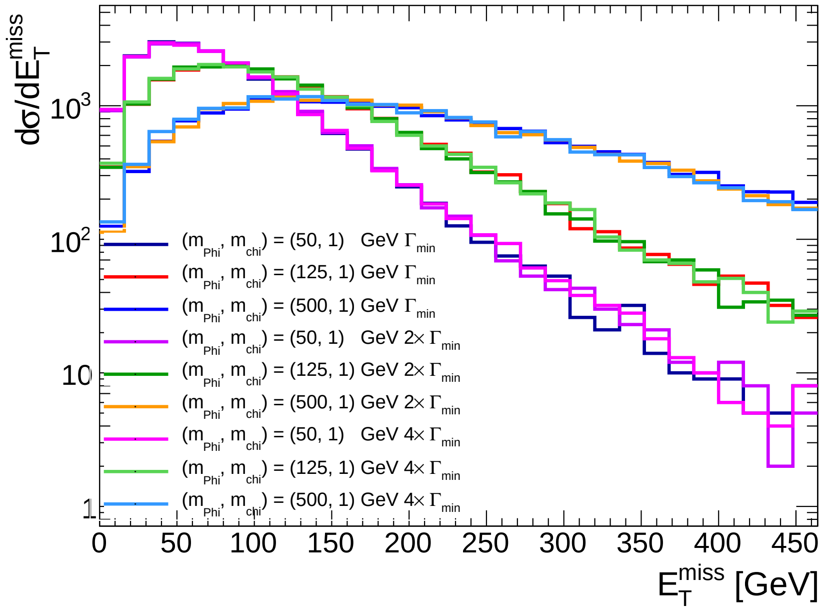

Figure 2.4: Study of the dependence of kinematics on the width of a scalar mediator. The width is increased up to four times the minimal width for each mediator and dark matter mass combination.

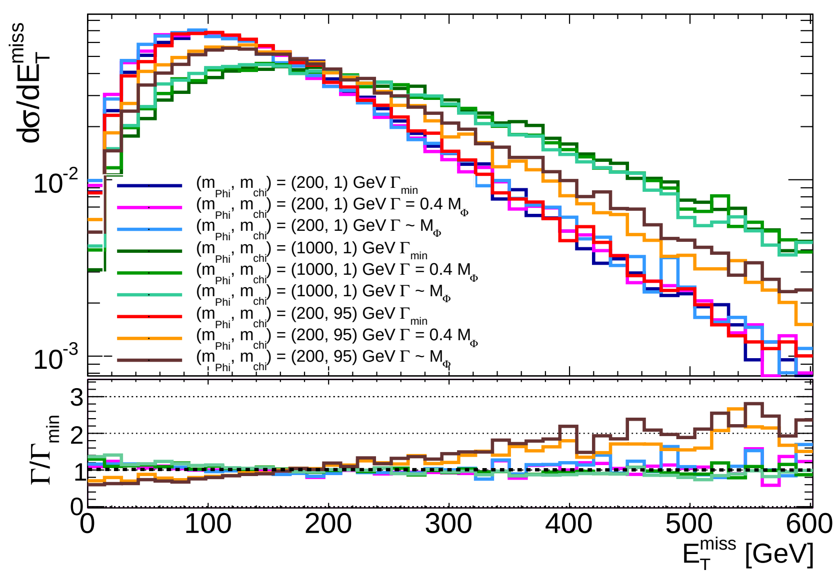

Figure 2.5: Dependence of the dependence of kinematics on the width of a scalar mediator. The width is increased up to the mediator mass. Choices of mediator and dark matter masses such that $m_{\phi,a}$ is slightly larger than $2m_\chi$ is the only case that shows a sizeable variation of the kinematics as a function of the width.

a limited range of coupling values (see Fig. 2.6 for example), we also choose to provide instead a table of cross section times branching ratio values over a large range of couplings to support interpretation of search results (see the Appendix ??). The table lists couplings from $g = 0.1$ to $g = 3.5$, where the upper limit is chosen to close to the perturbative limit.

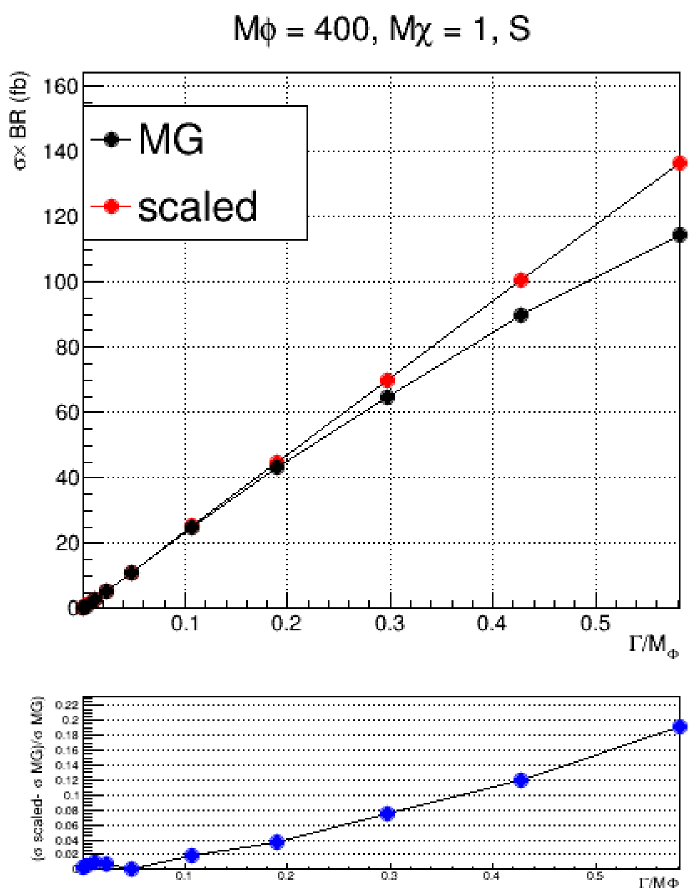

Figure 2.6: An example comparing a simple cross section scaling versus the computation from the generator, for a scalar model with $m_\phi = 400\,\text{GeV}$ and $m_{\text{DM}} = 1\,\text{GeV}$. In this example, the scaling relationship holds for Γ_ϕ / m_ϕ below 0.2, beyond which finite width effects become important and the simple scaling breaks down.

The points for the parameter scan chosen for this model are listed in Table 1.2, chosen to be harmonized with those for other analyses employing the same scalar model as benchmark. Based on the sensitivity considerations above, DM masses are only simulated up to 500 GeV, leading to a total of 24 benchmark points.

In addition to the considerations discussed in the preceding subsections, very light DM fermions are included ($m_{\text{DM}} = 10\,\text{GeV}$) as this is a region where colliders have a complementary sensitivity to current direct detection experiments.

Bibliography

[A+14] Jalal Abdallah et al. Simplified Models for Dark Matter and Missing Energy Searches at the LHC. *arXiv:1409.2893*, 2014.

[A+15] Georges Aad et al. Search for new phenomena in final states with an energetic jet and large missing transverse momentum in pp collisions at $\sqrt{s} = 8$ TeV with the ATLAS detector. 2015.

[ADR+14] Mohammad Abdullah, Anthony DiFranzo, Arvind Rajaraman, Tim M.P. Tait, Philip Tanedo, et al. Hidden on-shell mediators for the Galactic Center γ-ray excess. *Phys.Rev.*, D90(3):035004, 2014.

[ATL14] Sensitivity to WIMP Dark Matter in the Final States Containing Jets and Missing Transverse Momentum with the ATLAS Detector at 14 TeV LHC. Technical Report ATL-PHYS-PUB-2014-007, CERN, Geneva, Jun 2014.

[AWZ14] Haipeng An, Lian-Tao Wang, and Hao Zhang. Dark matter with t-channel mediator: a simple step beyond contact interaction. *Phys. Rev. D*, 89:115014, 2014.

[BB13] Yang Bai and Joshua Berger. Fermion Portal Dark Matter. *JHEP*, 11:171, 2013.

[BDSJ+14] Giorgio Busoni, Andrea De Simone, Thomas Jacques, Enrico Morgante, and Antonio Riotto. On the Validity of the Effective Field Theory for Dark Matter Searches at the LHC Part III: Analysis for the t-channel. *JCAP*, 1409:022, 2014.

[BFG15] Matthew R. Buckley, David Feld, and Dorival Goncalves. Scalar Simplified Models for Dark Matter. *Phys.Rev.*, D91(1):015017, 2015.

[CEHL14] Spencer Chang, Ralph Edezhath, Jeffrey Hutchinson, and Markus Luty. Effective WIMPs. *Phys. Rev. D*, 89:015011, 2014.

[CRTW14] Randel C. Cotta, Arvind Rajaraman, Tim M. P. Tait, and Alexander M. Wijangco. Particle Physics Implications and Constraints on Dark Matter Interpretations of the CDMS Signal. *Phys.Rev.*, D90(1):013020, 2014.

[DNRT13] Anthony DiFranzo, Keiko I. Nagao, Arvind Rajaraman, and Tim M. P. Tait. Simplified Models for Dark Matter Interacting With Quarks. *JHEP*, 1311, 2013.

[HKR13] Ulrich Haisch, Felix Kahlhoefer, and Emanuele Re. QCD effects in mono-jet searches for dark matter. *JHEP*, 1312:007, 2013.

[HR15] Ulrich Haisch and Emanuele Re. Simplified dark matter top-quark interactions at the LHC. 2015.

[PVZ14] Michele Papucci, Alessandro Vichi, and Kathryn M. Zurek. Monojet versus the rest of the world I: *t*-channel models. *JHEP*, 2014.